Journal of The Electrochemical Society

The Electrochemical Society
Advancing solid state & electrochemical science & technology

OPEN ACCESS

Effect of Light and Electrode Polarization on $BiVO_4$ and TiO_2 Photoanodes for Glycerol Oxidation

To cite this article: Martí Molera *et al* 2024 *J. Electrochem. Soc.* **171** 086503

View the article online for updates and enhancements.

You may also like

- Generation of Value-Added Products from Glycerol Oxidation by Pd Based Catalysts in Alkaline Medium
  Livia Martins Palma, Thiago Santos Almeida, Vanessa Luciane Oliveira et al.
- Highly Active PdAg/C Catalysts for the Electrooxidation of Propan-1-ol
  Nan Cai, Changchun Jin, Cuicui Wan et al.
- Improved Glycerol Electrooxidation at Carbon-Supported PdFe Bimetallic Catalysts
  Guilherme Bueno Bresciani, Jefferson Honorio Franco, K. Boniface Kokoh et al.

Watch Your Electrodes Breathe!

EL-CELL®
electrochemical test equipment

Measure the Electrode Expansion in the Nanometer Range with the ECD-4-nano.

✓ Battery Test Cell for Dilatometric Analysis (Expansion of Electrodes)
✓ Capacitive Displacement Sensor (Range 250 µm, Resolution ≤ 5 nm)
✓ Detect Thickness Changes of the Individual Half Cell or the Full Cell
✓ Additional Gas Pressure (0 to 3 bar) and Temperature Sensor (-20 to 80° C)

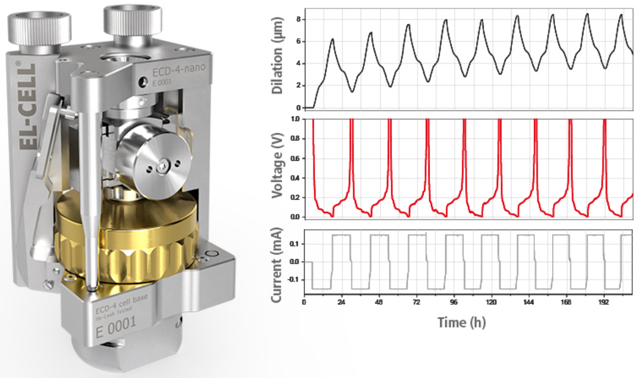

See Sample Test Results:
Scan me!

Download the Data Sheet (PDF):
Scan me!

Or contact us directly:
☎ +49 40 79012-734
sales@el-cell.com
www.el-cell.com

This content was downloaded from IP address 176.84.173.197 on 22/08/2024 at 09:49

Journal of The Electrochemical Society, 2024 **171** 086503

Effect of Light and Electrode Polarization on $BiVO_4$ and TiO_2 Photoanodes for Glycerol Oxidation

Martí Molera,[1,2] Maria Sarret,[1,2] Cristian Fàbrega,[2,3] and Teresa Andreu[1,2,z]

[1] *Departament de Ciència dels Materials i Química Física, Universitat de Barcelona (UB), Martí i Franquès 1, 08028 Barcelona, Spain*
[2] *Institut de Nanociència i Nanotecnologia (IN2UB), Universitat de Barcelona (UB), Martí i Franquès 1, 08028 Barcelona, Spain*
[3] *Departament d'Enginyeria Electrònica i Biomèdica, Universitat de Barcelona (UB), Martí i Franquès 1, 08028 Barcelona, Spain*

In recent years, there has been a growing interest in the photoelectrochemical oxidation of glycerol to produce high-value products. Most studies have focused solely on the photocatalytic properties of the electrodes, overlooking their electrocatalytic properties and the different products obtained under dark conditions. Our work aims to address this gap by comparing the electrocatalytic activity under dark and light conditions to determine whether light influences the reactivity of the electrodes or if it just reduces the overpotential of the reaction. To achieve this, we employed two model semiconductors, TiO_2 and $BiVO_4$. We have analyzed their polarization curves under both dark and light conditions and evaluated the competence of glycerol oxidation reaction with the oxygen evolution reaction. Furthermore, we conducted long-term (photo)electrolysis revealing the beneficial role of light on the electrolytic process, as it enables the obtention of C3 products on illuminated TiO_2 photoanodes at low electrode polarization, comparable to the performance of $BiVO_4$.

[DOI: 10.1149/1945-7111/ad6bc3]

Manuscript submitted March 25, 2024; revised manuscript received July 15, 2024. Published August 14, 2024.

Supplementary material for this article is available online

Hydrogen production is a key process as a future energy vector, yet the current production methods rely heavily on non-renewable sources such as steam reforming and coal gasification. As a result, there is a rising interest in water splitting as a green route of obtaining hydrogen. However, this process suffers from a high energetic cost mainly due to kinetic limitations in the oxygen evolution reaction (OER) resulting in a high overpotential.[1] One potential strategy for overcoming this challenge involves the oxidation of organic compounds with less demanding kinetics, which can reduce the overall energetic cost of the reaction.

Glycerol, an organic alcohol produced as a by-product of the biodiesel industry, stands out as a highly promising alternative to OER. With its production exceeding industry demands, it can be available at a price range between 0.68 $ and 0.95 $ per kg depending on the purity. This makes it a cost-effective feedstock for hydrogen production, since other feedstocks such as HMF or furfural have prices ranging from 0.78 $ to 1.12 $ per kg and 1.17 $ and 1.82 $ per kg respectively.[2–4] Additionally, glycerol can be oxidised to high-value molecules such as dihydroxyacetone or formic acid, enabling the commercialisation of the anodic products. However, implementing this process in the industry requires overcoming two main challenges: the reduction of the energy cost of the process and the enhancement of selectivity towards a specific product.

The use of semiconductor electrodes has been proposed as a means of reducing the energy expenditure of the process. This is achieved by harnessing solar radiation as an energy source with the incorporation of semiconductors such as titanium oxide (TiO_2)[5,6] or bismuth vanadate ($BiVO_4$)[7] in a photoelectrochemical (PEC) setup. TiO_2 is one of the most known photocatalysts due to its low cost and stability, with a bandgap of 3.1 eV. Its nanostructures have been extensively researched for various applications, including glycerol oxidation reaction (GOR).[5,6,8,9] Former studies pointed out that bare TiO_2 have poor selectivity towards GOR, requiring co-catalysts to obtain good performances.[10,11] Nonetheless, TiO_2 suffers from a limited solar light absorption, restricted to the use of UV light. Because of that, $BiVO_4$ has emerged as an alternative, being a photoactive n-type semiconductor with a bandgap of 2.4 eV with suitable conduction band edges to split water and potentially higher conversion efficiencies than TiO_2. Unfortunately, its maximum potential remains unrealized because it suffers from a high recombination rate.[7]

Recent studies have explored bare $BiVO_4$ under various conditions,[12–14] and several modifications have been proposed to enhance $BiVO_4$ performance. One strategy involves the fabrication of multi-layered electrodes to improve electron conductivity,[15–17] while another consists on introducing co-catalysts onto the surface.[14,18–24] All these studies have focused on the photocatalytic properties of the electrodes overlooking their inherent electrocatalytic properties. Furthermore, the different products obtained in dark conditions under the same kinetic regime has not been properly reported. In our study, we aim to address this gap by comparing the electrocatalytic activity of these materials under dark and light conditions. This work seeks to elucidate whether light influences the reactivity of the electrodes or if it just reduces the overpotential of the reaction.

Experimental

Synthesis of TiO_2 photoanodes.—TiO_2 layers were grown by hydrothermal synthesis on fluorine-doped tin oxide (FTO) conductive glass substrates (7 Ω/sq).[25] Prior to synthesis, substrates (2×5 cm^2) were cleaned with acetone, isopropanol and deionised (DI) water through sonication, followed by drying under a nitrogen stream. To prevent deposition on the edges and ensure subsequent electrical access to the FTO, Teflon tape was applied to mask the substrate. In a typical synthesis, a solution consisting of 0.915 g of $Ti(OBu)_4$ in 60 ml of 6 M HCl was introduced into a 150 ml Teflon vessel, with the substrate positioned at an inclination of 45° with the FTO side downwards. The vessel was then placed in a stainless-steel autoclave and heated to 180 °C for 6 h. Finally, the electrodes were rinsed with deionized water, dried, and annealed at 500 °C for 2 h to remove any superficial chlorides from the synthesis process.

Synthesis of $BiVO_4$ photoanodes.—To synthesize $BiVO_4$ electrodes an electrodeposition method followed by thermal treatment was followed.[26] Initially, BiOI was electrodeposited onto FTO-glass substrates by applying two potentiostatic pulses: one at −0.35 V *vs.* Ag/AgCl/KCl (3.5 M) for 1 minute, followed by another at −0.1 V *vs.* Ag/AgCl/KCl (3.5 M) for 3 minutes, using a Biologic VSP300

---

[z] E-mail: tandreu@ub.edu

potentiostat. To prepare the electrochemical bath, 0.97 g of $Bi(NO_3)_3$ and 3.32 g of KI were dissolved in 50 ml of water, to which a solution of 0.5 g of p-benzoquinone in 20 ml of ethanol was added. The BiOI electrodes were subsequently cleaned with deionised water and dried in air. Once dried, a drop of vanadium precursor solution (0.2 M vanadyl acetylacetonate in DMSO solvent) was added to the electrodes. Subsequently, the samples were heated for 2 h at 450 °C with a heating ramp of 2 °C min^{-1}. After cooling, excess V_2O_5 was removed by cleaning the electrodes with a 1 M KOH solution for 3 minutes, followed by rinsing with water and drying.

Characterisation.—The structural and optical properties of the $BiVO_4$ and TiO_2 electrodes were investigated using various techniques. The morphology of the samples were analysed via Field emission scanning electron microscopy (FESEM) on a JEOL J-7100 coupled with energy dispersive spectroscopy (EDS). X-ray diffraction (XRD) patterns were acquired using a PANalytical X'pert PRO diffractometer with monochromatized Cu Kα radiation ($\lambda = 1.5406$ Å), operating at 45 kV and 40 mA in a Bragg-Brentano configuration. Raman spectroscopy was conducted using a Jovin Yvon LabRaman HR800 in the 100–1000 cm^{-1} range employing a green laser (532 nm) and calibrated using a silicon reference. UV–vis spectroscopy (UV–vis) was performed on a Lambda 950 UV–vis-NIR spectrometer (PerkinElmer) equipped with a 150 mm Integrating Sphere and Spectralon standard. X-ray photoelectron spectroscopy (XPS) experiments were performed in a PHI 5500 Multitechnique System (from Physical Electronics) with a monochromatic X-ray source (Al K_α 1486.6 eV). Transmittance and reflection measurements were separately conducted for each sample in a wavelength range of 100–800 nm, with a step of 5 nm and the band gap was determined based on a Tauc plot.

Photoelectrochemical measurements.—Photoelectrochemical (PEC) measurements were conducted in a Hëllma large optical glass cuvette (20 ml). The electrolyte solution contained 0.5 M Na_2SO_4 with or without 0.1 M glycerol. The PEC tests were conducted at pH 2 and 7, adjusted with diluted H_2SO_4 or NaOH, to work with the completely protonated or deprotonated forms of the glycerol oxidation intermediates and products (Table S1). A three-electrode configuration was used, with a leak-free Ag/AgCl/KCl (3.5 M) (Innovative Instruments) as the reference electrode and a platinum filament (Heraeus) as the counter electrode. All potentials were converted to the reversible hydrogen electrode (RHE) using the Nernst equation considering E^0 (KCl/AgCl/Ag) = 0.205 V_{RHE}, following the Eq. 1.

$$E_{RHE} = E_{(KCl/AgCl/Ag)} + 0.205 + 0.059\,pH \qquad [1]$$

For photoelectrochemical measurements, the light source employed was a collimated Thorlabs high-power LED (385 nm) with an irradiance of 10 mW cm^{-2} on the sample measured with a Thorlabs S120VC silicon photodiode. The onset potentials were determined by employing the Tafel plot (E *vs.* log |j|), which allows to know the potential at which the photocurrent begins to rise, as described in Fig. S1. A SHB1T Thorlabs diaphragm shutter was employed when necessary. Electrochemical Impedance Spectroscopy (EIS) measurements were recorded under dark conditions in a frequency range of 100000–0.1 Hz and an amplitude of 10 mV.

Evaluation of glycerol oxidation products.—Long electrolysis and photoelectrolysis were conducted to assess product distribution. The photoelectrochemical cell utilized was a homemade Teflon cell (Fig. S2) with two compartments (3 ml each) separated by a Nafion 117 membrane. The electrolyte solution consisted of 0.5 M Na_2SO_4 with 0.1 M glycerol, adjusted to pH 2 or 7. Continuous stirring was maintained during (photo)electrolysis to prevent mass transport limitations. Control experiments were performed in the absence of glycerol. Each condition was replicated at least twice. For each product, the faradaic efficiency was calculated according to Eq. S1 in the supplementary information.

Photoelectrolysis experiments were conducted at a constant potential, typically 1 V_{RHE}, with light irradiance regulated to achieve a photocurrent within the range of 2–2.5 mA cm^{-2}. Dark electrolysis was carried out under galvanostatic conditions at 2 mA cm^{-2}. In both cases, the charge was limited to 7.5, 15 or 22.5 C (2.5–5.0–7.5 C ml^{-1}). After electrolysis, the electrolyte sample from the anode compartment was kept in a fridge until it was analysed by high-performance liquid chromatography (HPLC) and nuclear magnetic resonance (NMR) to determine the faradaic efficiency. HPLC analysis was conducted using a Waters Alliance e2695 cromatograph with an Aminex HPLX-87H carboxylic acid column at 60 ° C, with a sample loop of 100 μl. Diluted sulfuric acid (10 mM) was used as the mobile phase at a flow rate of 0.6 ml min^{-1}. The products were detected with a Jasco UV-1570 UV–vis spectrophotometer and a Waters 2414 refractive index detector. H-NMR analysis was carried out on a Bruker 400 instrument, with a water suppression method.[27] For sample preparation, 490 μl of the sample was mixed with 90 μl of deuterium oxide and 20 μl of 0.2%vol DMSO as an internal standard.

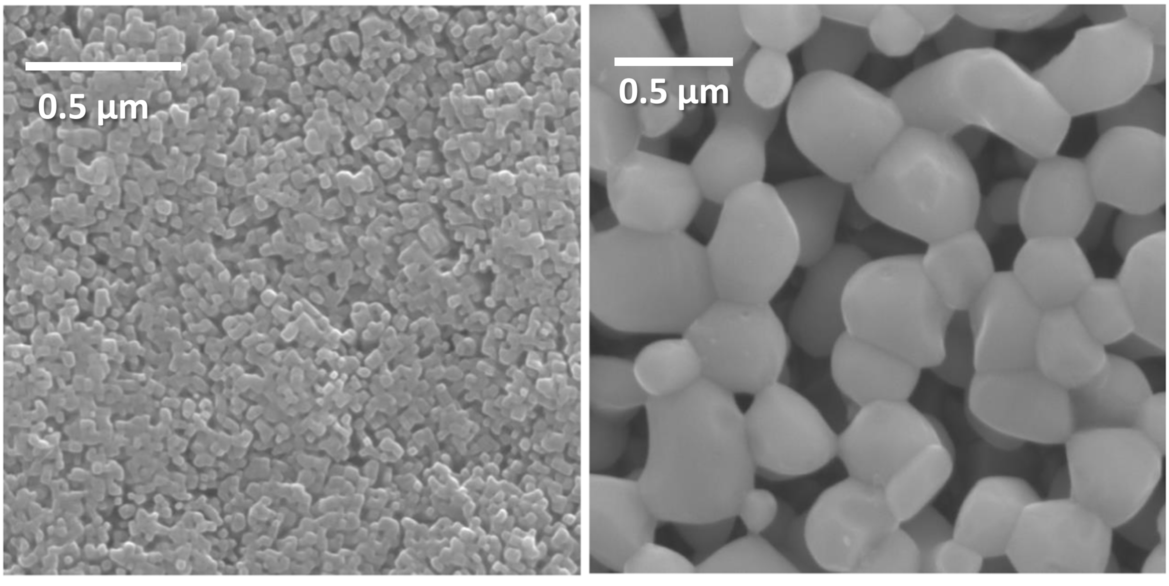

Figure 1. FESEM images of TiO_2 (left) and $BiVO_4$ (right) photoanodes.

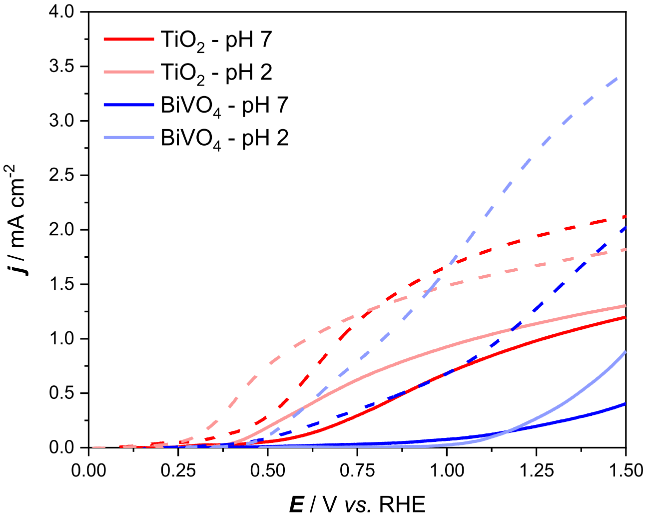

Figure 2. LSV curves recorded at a scan rate of 5 mV s^{-1} in 0.5 M Na_2SO_4 electrolyte (pH 2 and 7) for OER (full line) and with added 0.1 M glycerol for GOR (dotted line) conditions, under 10 mW cm^{-2} illumination.

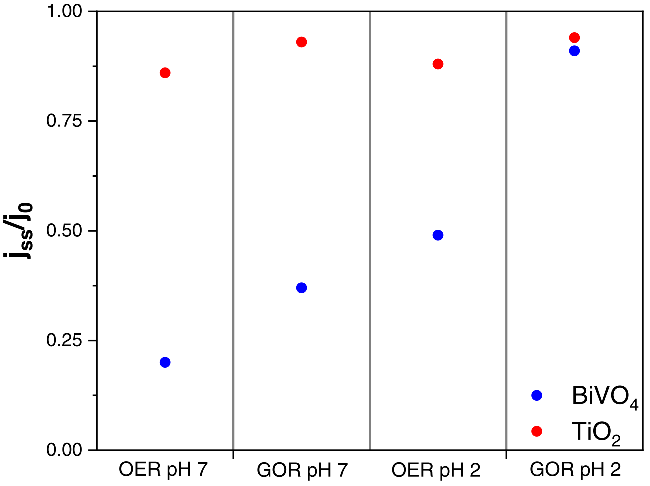

Figure 3. j_{ss}/j_0 ratio in OER conditions (0.5 M Na_2SO_4) and GOR conditions (0.5 M Na_2SO_4 + 0.1 M glycerol) under acidic (pH2) and neutral (pH7). Transient photocurrent acquired under potentiostatic conditions at 1 V_{RHE}, with chopped light at a frequency of 50 mHz.

Results and Discussion

Structural characterisation.—The FESEM images presented in Figs. 1 and S3 reveal the highly porous nature of both samples, suggesting a high active surface area. $BiVO_4$ exhibits a wormlike structure composed of interconnected small grains (<0.5 μm) while TiO_2 presents a more compact structure, characterised by a dense layer (<0.1 μm) of square-section nanorods. Further analysis (Table S2) using EDS indicates the absence of major impurities in both materials. The XRD patterns (Fig. S4) of $BiVO_4$ and TiO_2 closely match the monoclinic $BiVO_4$ patterns (JCPDS 00–014–0688) and the rutile TiO_2 patterns (JCPDS 00–021–1276). $BiVO_4$ presents the typical peak distribution in its XRD pattern, indicating no preferential orientation. In contrast, TiO_2 shows a preferential growth by presenting only six peaks corresponding to the planes (101), (111), (211), (002), (301) and (112), with the (101) plane being most prominent. Raman spectroscopy (Fig. S5) further confirms the monoclinic structure of $BiVO_4$ with bands at 826 cm^{-1}, 365 cm^{-1}, 326 cm^{-1}, 208 cm^{-1} and 126 cm^{-1}.[28–30] The 826 cm^{-1} band is attributed to the symmetric V-O stretching mode (A_g), while the 365 cm^{-1} and 326 cm^{-1} bands correspond to the symmetric (A_g) and antisymmetric (B_g) V-O bending modes of VO_4. Lastly, the 208 cm^{-1} and 126 cm^{-1} bands correspond to the external rotation and translation modes. On the other hand, TiO_2 exhibits characteristic bands of rutile at 610 cm^{-1}, 446 cm^{-1}, and 143 cm^{-1}.[31,32] The 610 cm^{-1} band is attributed to the symmetric stretching of the O-Ti-O bonds in the (110) plane (A_{1g}), while the 446 cm^{-1} band corresponds to the asymmetric bending of the O-Ti-O bonds in the (001) plane (E_g). Finally, the 143 cm^{-1} band is attributed to a combination of the asymmetric bending of the O-Ti-O bonds in the planes (001), (110) and (−110) (B_{1g}). XPS analysis was performed to confirm the chemical structure of the materials. As can be seen in Fig. S6, both survey spectra do not present any iodine (619–620 eV) or chlorine (199–200 eV) elements, confirming the successful removal of the chemical precursors during the calcination process of $BiVO_4$ and TiO_2 photoanodes synthesis. In both materials, the O 1 s spectra presents two contributions, one centered at 529.6 eV corresponding to the oxygen lattice (M-O-M) and a second one at 531.6–532.1 eV corresponding to the characteristic surface hydroxyls (M-OH) of metal oxides exposed to water.[33] In the case of $BiVO_4$, the Bi 4 f spectrum shows a doublet at 159.0 eV and 164.3 eV, for Bi $4f_{7/2}$ and Bi $4f_{5/2}$, in agreement with the presence of Bi^{3+}. The V 2p region corresponds to the binding energies of V^{5+}, located at 516.5 eV and 524.2 eV for V $2p_{3/2}$ and V $2p_{1/2}$.[34] In the case of TiO_2, the peaks at 458.3 eV and 464.0 eV are ascribed to Ti $2p_{3/2}$ and Ti $2p_{1/2}$ of the Ti^{4+} oxidation state.[35] Furthermore, UV–vis analysis (Fig. S7) was conducted to determine the band gap of $BiVO_4$ and TiO_2, yielding values of 2.46 eV and 2.95 eV, respectively.

Photoelectrochemical characterisation.—Initially, we investigated the photoelectrodes under illumination conditions. Figure 2 presents the linear sweep voltammograms of both photoanodes in the absence and presence of 0.1 M glycerol, aiming to assess the competition between water oxidation (oxygen evolution reaction, OER) and glycerol oxidation reaction (GOR) under neutral (pH 7) and acidic (pH 2) electrolytes.

For GOR, TiO_2 electrodes attain a photocurrent of 1.5 mA cm^{-2} at 1 V_{RHE} with an onset potential of 0.08 V_{RHE} at pH 2 and a photocurrent of 1.7 mA cm^{-2} at 1 V_{RHE} with an onset potential of 0.07 V_{RHE} at pH 7. Meanwhile, for the OER, a photocurrent of 0.92 mA cm^{-2} at 1 V_{RHE} with an onset potential of 0.30 V_{RHE} at pH 2 and a photocurrent of 0.7 mA cm^{-2} at 1 V_{RHE} with an onset potential of 0.22 V_{RHE} at pH 7 are achieved. From the linear sweep voltammetry (LSV) depicted in Fig. 2, it is evident that acidic conditions reduce the overpotential of the reaction at low polarizations. However, at electrode potentials exceeding 0.8 V_{RHE}, there is a shift in reaction kinetics, leading to higher photocurrents under neutral conditions. It is worth noting that for TiO_2, the photocurrent for OER exhibits high intensity, suggesting a potential competition between OER and GOR at 1 V_{RHE}, which could potentially reduce the overall efficiency of glycerol oxidation.

For $BiVO_4$ electrodes, acidic conditions are optimal for GOR, as evidenced by a photocurrent of 1.64 mA cm^{-2} at 1 V_{RHE} with an onset potential of 0.35 V_{RHE} at pH 2, compared to a photocurrent of 0.65 mA cm^{-2} at 1 V_{RHE} with an onset potential of 0.22 V_{RHE} at pH 7. Interestingly, $BiVO_4$ electrodes exhibit a markedly different behaviour than TiO_2. Specifically, under acidic conditions, similar photocurrents are reached at 1 V_{RHE} for both electrodes, albeit with a negligible contribution of OER in the case of $BiVO_4$ photoanodes, indicating a prevalence of GOR over OER. Under neutral conditions $BiVO_4$ photoanodes also show no significant OER contribution at 1 V_{RHE} but present lower photoelectrochemical efficiency.

In summary, TiO_2 and $BiVO_4$ exhibit distinct behaviours regarding glycerol oxidation reaction (GOR). TiO_2 photoanodes tend to generate a high photovoltage, thereby reducing the overpotential, but they face significant competition from oxygen evolution reaction (OER). Conversely, $BiVO_4$ photoanodes encounter difficulty in achieving high photocurrents at low polarization values

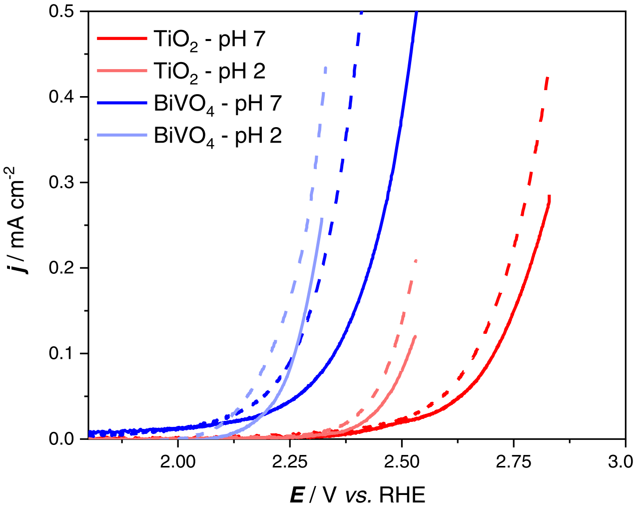

Figure 4. LSV curves recorded at a scan rate of 5 mV s^{-1} in 0.5 M Na_2SO_4 electrolyte (pH 2 and 7) for OER (full line) and with added 0.1 M glycerol for GOR (dotted line) conditions. Dark conditions.

but demonstrate significantly greater efficiency for GOR compared to OER.

As previously mentioned, one of the main limitations of $BiVO_4$ is its high recombination rate, which is favoured by the sluggish kinetics towards the oxygen evolution reaction.[36] This is clearly apparent when analysing the photocurrent transients under potentiostatic chopped illumination. The ratio between the steady-state photocurrent and the initial photocurrent (j_{ss}/j_0) provides an estimate of the surface electron-hole recombination losses. As shown in Fig. 3, TiO_2 exhibits high charge carrier extraction, with minimal recombination, maintaining a stable photocurrent over time for OER, with a j_{ss}/j_0 ratio greater than 0.86, which is moderately improved in the presence of glycerol. Glycerol can be easily oxidised and is frequently used as a hole scavenger for photocatalytic processes.[37] Consequently, in all cases the j_{ss}/j_0 ratio increases due to the facilitated hole extraction, which mitigates the recombination of the photogenerated charges at semiconductor/electrolyte interface. Therefore, the transient photocurrents of $BiVO_4$ are significantly influenced by the conditions. At both pH environments, the presence of glycerol enhances the j_{ss}/j_0 ratio by 85%. Moreover, in accordance with the differences observed in the linear sweep voltammetry under illumination, acidic media also plays a role in preventing recombination, both for OER and GOR, resulting in j_{ss}/j_0 values comparable to TiO_2, thus ensuring efficient hole extraction for $BiVO_4$ photoanodes.

Lastly, we conducted electrochemical measurements in the dark, where Fig. 4 reveals a reverse trend compared to illumination conditions. While the onset potentials for illuminated TiO_2 photoanodes were lower than those of $BiVO_4$, the electrocatalytic overpotentials for TiO_2 electrodes are higher than for $BiVO_4$, consistent with the expected photovoltages. In the case of TiO_2, with a larger bandgap, the photovoltage was around 2.1 V, whereas for $BiVO_4$ it was around 1.6 V. Moreover, comparing both electrolytes, GOR appears to be favoured in acidic conditions, as observed under illumination conditions. This was corroborated by EIS analysis (Figs. S8 and S9), where it can be seen that the charge transfer resistance (R_{CT}) is lower in acidic conditions in both $BiVO_4$ and TiO_2 electrodes.

In addition to the inherent decrease in the working electrode potential under illumination conditions, which lowers the energy expenditure of the process, there is a change in the separation of the OER and GOR potentials when the illumination variable is considered. Under dark conditions, the electrode potential difference between glycerol oxidation reaction (GOR) and oxygen evolution reaction (OER) is considerably lower for both materials (100 mV for $BiVO_4$ and 45 mV for TiO_2) compared to illumination conditions (650 mV for $BiVO_4$ and 250 mV for TiO_2). Additionally, EIS analysis also showed that the difference in R_{CT} between OER and GOR was higher for $BiVO_4$ electrodes. This suggests that illumination not only enables GOR at lower overpotentials but reduces the competitiveness between GOR and OER, which may have an impact on faradaic efficiency.

Glycerol photoelectrochemical valorisation.—To analyse the product distribution of glycerol oxidation reaction, we conducted long electrolysis and photoelectrolysis using both semiconductors, under similar kinetic regimes. Glycerol can be oxidised into a wide

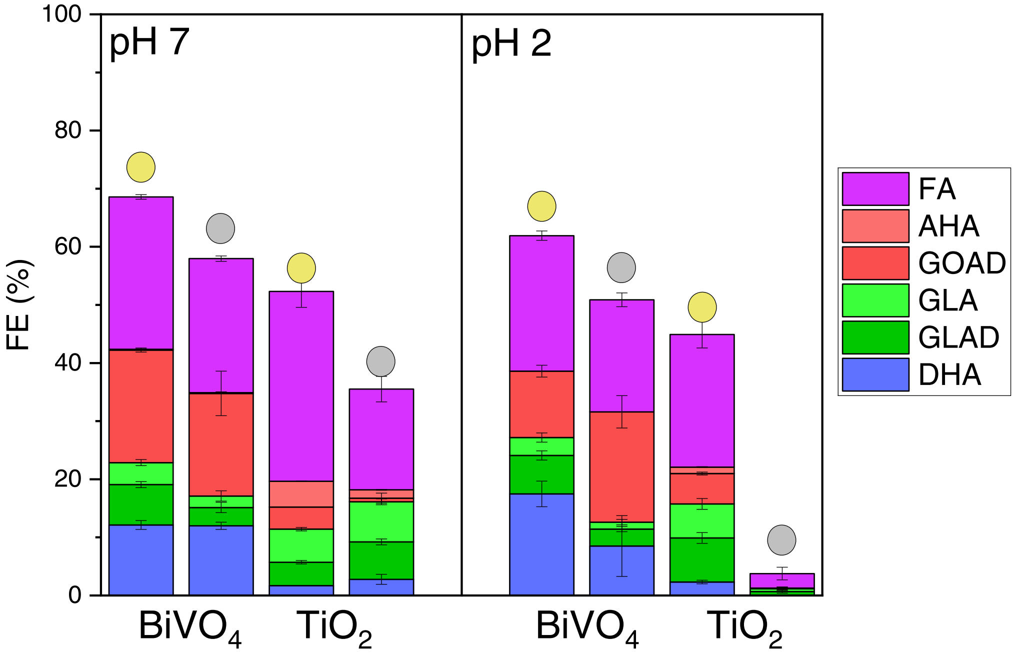

Figure 5. Faradaic efficiencies for glycerol oxidation. The yellow dot is for potentiostatic photoelectrolysis at 1 V_{RHE}. The grey dot corresponds to galvanostatic dark electrolysis at 2 mA cm^{-2}.

variety of products, depending on the degree of oxidation. We can obtain dihydroxyacetone (DHA), glyceraldehyde (GLAD) and glyceric acid (GLA) as C3 products, hydroxyacetic acid(AHA) and glycolaldehyde (GOAD) as C2 products, formic acid (FA) as a C1 product, up to the complete mineralization to carbon dioxide. Figure 5 shows the faradaic efficiencies of both materials and electrolytes, after potentiostatic photoelectrolysis and galvanostatic dark electrolysis.

Upon closer examination of the results, we observe distinct behaviours between the two semiconductors. Generally, $BiVO_4$ exhibits higher faradaic efficiencies compared to TiO_2, partially attributed to the anticipated competition between OER and GOR in TiO_2 samples as discussed in the photoelectrochemical LSV measurements. However, for $BiVO_4$ photoanodes, FE losses cannot solely be attributed just to competition with OER, indicating that there is a second parasitic reaction in the form of the overoxidation of glycerol to CO_2. In Fig. S10 we can see that over time there is no change in faradaic efficiency and selectivity for any of the photoelectrolysis conducted. This suggests that the measured products are not intermediates of the reaction nor subject to degradation in other parasitic reactions.

Regarding the distribution of glycerol oxidation products, we found differences between $BiVO_4$ and TiO_2 photoelectrodes. As seen in Fig. S11 $BiVO_4$ acts as a moderate oxidant with a higher tendency towards producing C3 and C2 products, while TiO_2 tends to favour the formation of highly oxidised C1 products (formic acid). This suggests that on $BiVO_4$, although glycerol can be completely oxidised to CO_2, the oxidation products have lower surface adsorption and tend to desorb at all stages of electrolysis, leading to this product distribution. Conversely, the adsorption of oxidation products on the TiO_2 electrode is much stronger, favouring formic acid production.[7,10,13] Additionally, in TiO_2 electrolysis there is an additional reaction pathway towards the formation of hydroxyacetic acid (AHA). When comparing $BiVO_4$ samples at different pH levels, an increase of C3 and decrease of C2 and C1 products can be observed in acidic media, indicating that acidity influences the adsorption of intermediary species. However, the distribution of the products on TiO_2 photoanodes is less influenced by pH variations.

In all cases, dark electrolysis results in a lower faradaic efficiency compared to illumination conditions, in agreement with the competition between OER and GOR. As discussed earlier, for TiO_2, the difference in electrode potential between glycerol LSV and water oxidation is lower than 50 mV. Consequently, as glycerol is consumed, the electrode potential during electrolysis increases towards the OER, significantly reducing faradaic efficiency under dark conditions. Conversely, for $BiVO_4$, which exhibits a higher separation between GOR and OER electrode potentials, the faradaic efficiency values are closer to those under illumination, although they remain 10% lower than under illumination.

Polarization effects on product selectivity.—Plainpan, et al.[38] have proposed an alternative methodology to investigate complex photoelectrochemical systems with competitive reactions by plotting the differential of the linear sweep voltammetry measurements. The derivative voltammograms are proportional to the density of intermediary surface states (iSS) as a function of the applied potential. This data enables the identification of different reactions occurring simultaneously at the electrode surface. As depicted in Fig. S12, for $BiVO_4$, the derivative voltammetry of GOR presents two distinctive peaks, one centred at 0.55 V_{RHE} (Bi-SS1), corresponding to glycerol oxidation, and a second at 1 V_{RHE} (Bi-SS2). In the OER derivative voltammetry a 3rd iSS can be appreciated starting at 1.05 V_{RHE} (Bi-SS3), which would correspond to water oxidation. This indicates that there are two different iSS that are capable of oxidizing glycerol before the OER is relevant. Conversely, for TiO_2, there is only 1 peak, located at 0.4 V_{RHE} (Ti-SS1), associated with glycerol photoxidation, as the following broad band matches the peak of the OER derivative voltammogram centred at 0.6 V_{RHE} (Ti-SS2). Since previous photoelectrolysis experiments were conducted at 1 V_{RHE}, additional photoelectrolysis were carried out at the potentials where the iSS were located, 0.55 V_{RHE} for $BiVO_4$ and 0.4 V_{RHE} for TiO_2.

In Figs. 6 and S13, we observe that for TiO_2, at low potential (0.4 V_{RHE}), there is already some presence of the Ti-SS2 and thus competition between OER and GOR is already present, leading to a slight decrease in faradaic efficiency (FE) as OER becomes more prevalent. Regarding product selectivity, there is a significant

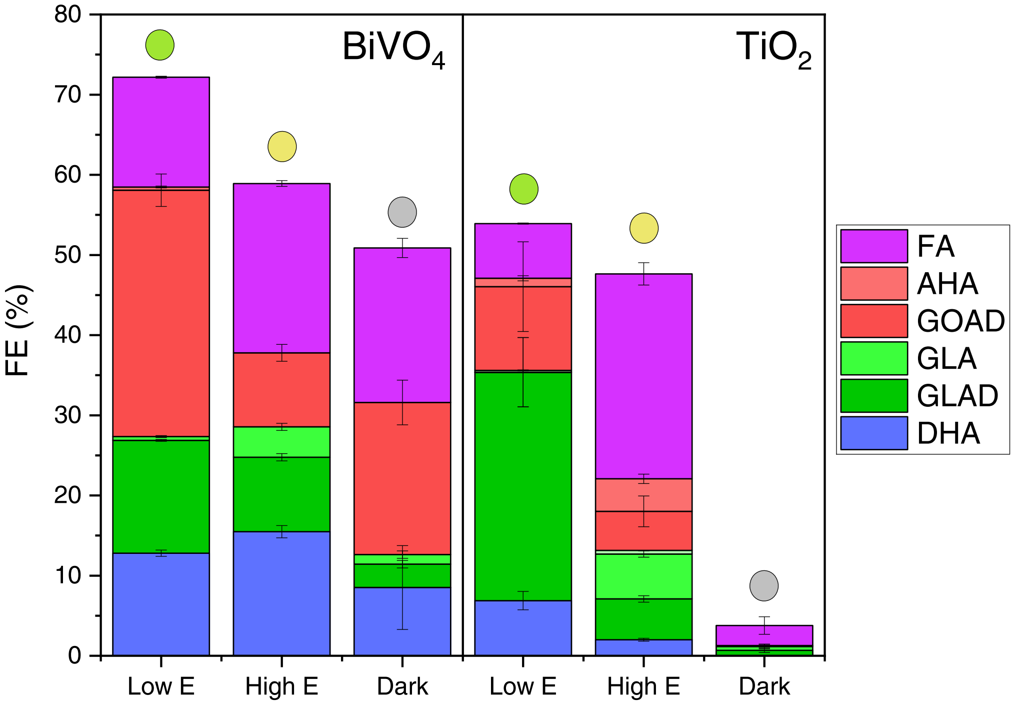

Figure 6. Faradaic efficiencies of oxidation products at 2 mA of intensity in variable conditions of potential and ilumination. Faradaic efficiencies for glycerol oxidation at pH 2. Green dot is for potentiostatic photoelectrolysis at low potential (0.55 V_{RHE} for $BiVO_4$ and 0.4 V_{RHE} for TiO_2). The yellow dot is for potentiostatic photoelectrolysis at a higher potential (1 V_{RHE}). The grey dot corresponds to galvanostatic dark electrolysis at 2 mA cm^{-2}.

increase in C3 species production at low potential, whereas at higher potentials, formic acid production is favoured. This indicates that glycerol oxidation is carried out in two steps, each mediated by a different iSS. Ti-SS1 is responsible for the oxidation of glycerol to glyceraldehyde, and the Ti-SS2 is responsible for the oxidation of glyceraldehyde to formic acid, as well as for water oxidation. In the case of $BiVO_4$, when passing from the Bi-SS1 to the Bi-SS2 we observe that C3 products remain constant, while glycolaldehyde decreases and formic acid slightly increases. This suggests that in $BiVO_4$, glycerol oxidation is also mediated by two different iSS. Bi-SS1 is responsible for the oxidation of glycerol to glycolaldehyde, Bi-SS2 is responsible for the oxidation from glycolaldehyde to CO_2, and Bi-SS3 is responsible for water oxidation. In conclusion, the applied polarization has a significant impact on the product selectivity. At higher potential, the more oxidative iSS (Ti-SS2 and Bi-SS2) will be catalysing the reaction towards complete mineralization, while lower potential iSS (Ti-SS1 and Bi-SS2) will halt the glycerol oxidation at C3 and C2 products.

Conclusions

In this work, we synthesized monoclinic $BiVO_4$ and rutile TiO_2 semiconductor photoelectrodes, aiming to assess their electrocatalytic activity for glycerol oxidation under both dark and light conditions. By analysing the polarization curves of both photoanodes in the presence and absence of glycerol, along with evaluating the faradaic efficiencies of the glycerol oxidation products we conclude that light has a beneficial effect on the electrolytic process. On one hand, it decreases the energy expenditure of the process by reducing the working electrode potential under illumination conditions. On the other hand, it has an impact on the faradaic efficiency since light has a lower degree of OER enhancement, thereby promoting glycerol oxidation. Finally, we found that by decreasing the electrode polarization an increase in overall faradaic efficiency can be attained, with a reduced tendency for formic acid formation. Notably, operating at low polarizations, close to OER onset photopotential, significantly enhances the C3 faradaic efficiency for TiO_2 photoanodes, comparable to the performance of $BiVO_4$.

Acknowledgments

The financial support from Ministerio de Ciencia e Innovación through projects PID2019–108136RB-C33, PID2022–138491OB-C33 (MICIU/AEI/10.13039/501100011033) and from AGAUR-Generalitat de Catalunya (2021SGR00712, 2024 FI-1 00421) are gratefully acknowledged. Authors thank Centres Científics i Tecnològics (CCiTUB), Universitat de Barcelona for the expert and technical help on XPS, Raman, FESEM, HPLC and H-NMR techniques and to Dr. Julià Lopez Vidrier the access to the UV–vis equipment.

ORCID

Martí Molera https://orcid.org/0000-0002-7210-981X
Maria Sarret https://orcid.org/0000-0003-4126-7142
Cristian Fàbrega https://orcid.org/0000-0001-8337-4056
Teresa Andreu https://orcid.org/0000-0002-2804-4545

References

1. M. G. Walter, E. L. Warren, J. R. McKone, S. W. Boettcher, Q. Mi, E. A. Santori, and N. S. Lewis, *Chem. Rev.*, **110**, 6446 (2010).
2. T. Attarbachi, M. D. Kingsley, and V. Spallina, *Fuel*, **340**, 127485 (2023).
3. T. Kahlstorf, J. N. Hausmann, T. Sontheimer, and P. W. Menezes, *Global Challenges*, **7**, 2200242 (2023).
4. M. G. Davidson, S. Elgie, S. Parsons, and T. J. Young, *Green Chem.*, **23**, 3154 (2021).
5. S. Çetinkaya, G. Khamidov, L. Özcan, L. Palmisano, and S. Yurdakal, *J. Environ. Chem. Eng.*, **10**, 107210 (2022).
6. W. Wang, J. Dong, X. Ye, Y. Li, Y. Ma, and L. Qi, *Small*, **12**, 1469 (2016).
7. L. W. Huang, T. G. Vo, and C. Y. Chiang, *Electrochim. Acta*, **322**, 134725 (2019).
8. T. T. Li, B. Shan, W. Xu, and T. J. Meyer, *ChemSusChem*, **12**, 2402 (2019).
9. M. J. Paik, J. W. Yoo, J. Park, E. Noh, H. Kim, S. G. Ji, Y. Y. Kim, and S. Il Seok, *ACS Energy Lett.*, **122**, 1864 (2022).
10. L. Luo et al., *J. Am. Chem. Soc.*, **144**, 7720 (2022).
11. Y. Liu, M. Wang, B. Zhang, D. Yan, and X. Xiang, *ACS Catal.*, **12**, 6946 (2022).
12. T. G. Vo, C. C. Kao, J. L. Kuo, C. Chau Chiu, and C. Y. Chiang, *Appl. Catal. B*, **278**, 119303 (2020).
13. D. Liu, J. C. Liu, W. Cai, J. Ma, H. B. Yang, H. Xiao, J. Li, Y. Xiong, Y. Huang, and B. Liu, *Nat. Commun.*, **10**, 1779 (2019).
14. Y. H. Wu, D. A. Kuznetsov, N. C. Pflug, A. Fedorov, and C. R. Müller, *J. Mater. Chem. A Mater.*, **9**, 6252 (2021).
15. P. M. Rao, L. Cai, C. Liu, I. S. Cho, C. H. Lee, J. M. Weisse, P. Yang, and X. Zheng, *Nano Lett.*, **14**, 1099 (2014).
16. L. P. Li, M. Liu, and W. D. Zhang, *J. Solid State Electr.*, **22**, 2569 (2018).
17. S. Lee et al., *ACS Appl. Mater. Interfaces*, **11**, 44069 (2019).
18. B. He, F. Zhao, P. Yi, J. Huang, Y. Wang, S. Zhao, Z. Li, Y. Zhao, and X. Liu, *ACS Appl. Mater. Interfaces*, **13**, 48901 (2021).
19. H. Tateno, S. Y. Chen, Y. Miseki, T. Nakajima, T. Mochizuki, and K. Sayama, *ACS Sustain Chem. Eng.*, **10**, 7586 (2022).
20. D. A. Reddy, Y. Kim, H. S. Shim, K. A. J. Reddy, M. Gopannagari, D. Praveen Kumar, J. K. Song, and T. K. Kim, *ACS Appl. Energy Mater.*, **3**, 4474 (2020).
21. J. A. Seabold and K. S. Choi, *J. Am. Chem. Soc.*, **134**, 2186 (2012).
22. X. Lu, K. Hang Ye, S. Zhang, J. Zhang, J. Yang, Y. Huang, and H. Ji, *Chem. Eng. J.*, **428**, 131027 (2022).
23. M. Zhao, T. Chen, B. He, X. Hu, J. Huang, P. Yi, Y. Wang, Y. Chen, Z. Li, and X. Liu, *J. Mater. Chem. A Mater.*, **8**, 15976 (2020).
24. Y. Han, M. Chang, Z. Zhao, F. Niu, Z. Zhang, Z. Sun, L. Zhang, and K. Hu, *ACS Appl. Mater. Interfaces*, **15**, 11678 (2023).
25. C. Fàbrega, D. Monllor-Satoca, S. Ampudia, A. Parra, T. Andreu, and J. R. Morante, *J. Phys. Chem. C*, **117**, 20517 (2013).
26. K. J. McDonald and K. S. Choi, *Energy Environ. Sci.*, **5**, 8553 (2012).
27. T. Chatterjee, E. Boutin, and M. Robert, *Dalton Trans.*, **49**, 4257 (2020).
28. H. M. Zhang, J. B. Liu, H. Wang, W. X. Zhang, and H. Yan, *J. Nanopart. Res.*, **10**, 767 (2008).
29. J. Yu and A. Kudo, *Adv. Funct. Mater.*, **16**, 2163 (2006).
30. G. Li, Y. Bai, and W. F. Zhang, *Mater. Chem. Phys.*, **136**, 930 (2012).
31. Y. Zhang, C. X. Harris, P. Wallenmeyer, J. Murowchick, and X. Chen, *J. Phys. Chem. C*, **117**, 24015 (2013).
32. V. Swamy, *Phys. Rev. B*, **77**, 195414 (2008).
33. H. Idriss, *Surf. Sci.*, **712**, 121894 (2021).
34. C. Yang, C. Qin, J. Zhong, J. Li, S. Huang, Q. Wang, and L. Ma, *J. Alloys Compd.*, **890**, 161883 (2022).
35. C. Ros, C. Fàbrega, D. Monllor-Satoca, M. D. Hernández-Alonso, G. Penelas-Pérez, J. R. Morante, and T. Andreu, *J. Phys. Chem. C*, **122**, 3295 (2018).
36. W. Zhu, Y. Yuan, and Y. Ma, *Sustain Energy Fuels*, **8**, 1077 (2024).
37. K. G. G. C. De Silva, M. Finale, and S. Chowdhury, *Mater. Res. Bull.*, **152**, 111834 (2022).
38. N. Plainpan, F. Boudoire, and K. Sivula, *Sustain Energy Fuels*, **6**, 3926 (2022).